Identification and characterization of influenza variants resistant to a viral endonuclease inhibitor

Min-Suk Song[a,1,2], Gyanendra Kumar[b,1], William R. Shadrick[c], Wei Zhou[d], Trushar Jeevan[a], Zhenmei Li[b], P. Jake Slavish[c], Thomas P. Fabrizio[a], Sun-Woo Yoon[a], Thomas R. Webb[d,3], Richard J. Webby[a,3], and Stephen W. White[b,3]

[a]Department of Infectious Diseases, St. Jude Children's Research Hospital, Memphis, TN 38105; [b]Department of Structural Biology, St. Jude Children's Research Hospital, Memphis, TN 38105; [c]Department of Chemical Biology and Therapeutics, St. Jude Children's Research Hospital, Memphis, TN 38105; and [d]Bioscience Division, SRI International, Menlo Park, CA 94025

Edited by Stephen Cusack, European Molecular Biology Laboratory, Grenoble, France, and accepted by the Editorial Board February 8, 2016 (received for review October 6, 2015)

The influenza endonuclease is an essential subdomain of the viral RNA polymerase. It processes host pre-mRNAs to serve as primers for viral mRNA and is an attractive target for antiinfluenza drug discovery. Compound L-742,001 is a prototypical endonuclease inhibitor, and we found that repeated passaging of influenza virus in the presence of this drug did not lead to the development of resistant mutant strains. Reduced sensitivity to L-742,001 could only be induced by creating point mutations via a random mutagenesis strategy. These mutations mapped to the endonuclease active site where they can directly impact inhibitor binding. Engineered viruses containing the mutations showed resistance to L-742,001 both in vitro and in vivo, with only a modest reduction in fitness. Introduction of the mutations into a second virus also increased its resistance to the inhibitor. Using the isolated wild-type and mutant endonuclease domains, we used kinetics, inhibitor binding and crystallography to characterize how the two most significant mutations elicit resistance to L-742,001. These studies lay the foundation for the development of a new class of influenza therapeutics with reduced potential for the development of clinical endonuclease inhibitor-resistant influenza strains.

virus | infection | replication | mutation | diketo acid

Influenza A viruses cause disease in a variety of species including humans (1). Seasonal influenza viruses infect 5–20% of the human population annually, and studies using data collected during the 1990s estimated that an average of 36,000 influenza related mortalities occurred each year in the United States alone (2). Vaccines are currently the first line of defense against seasonally circulating influenza viruses, and given their relative effectiveness, it is perhaps not surprising that innovative antiinfluenza drug discovery has not been considered a high priority by government or commercial interests. However, vaccine efficacy is limited by changes in the circulating viruses and by waning protection in the elderly (3, 4). Seasonal vaccines are also predicted to have limited efficacy against zoonotic strains that represent a serious and ongoing threat to human health. The recent 2009 pandemic showed that effective matching vaccines are unlikely to be available during the first wave of a pandemic (5). There have been four influenza pandemics within the past 100 y, including the devastating H1N1 outbreak in 1918 (6) and the H1N1 outbreak in 2009 (7). Although zoonotic avian viruses of the H5N1, H7N3, H7N7, H7N9, H9N2, and H10N8 subtypes have failed to spread in humans, fatality rates have approached 60% for some of these outbreaks (8, 9). Mutations that can facilitate human transmission of these zoonotic viruses are being identified (10, 11).

Subtype independent antiviral drugs represent excellent alternative antiinfluenza therapies. Historically, the development of effective antiviral therapies has been successful for the treatment of diseases caused by the HIV (12) and the Hepatitis C virus (HCV) (13). Considering that HIV and HCV diseases were considered to be "untreatable" in the not so distant past, the current treatment regimens are remarkably effective and can even lead to complete cures in the case of HCV. An attractive antiinfluenza drug target is the viral RNA-dependent RNA polymerase (RdRp) that synthesizes both genomic RNA and viral mRNA (14, 15). The recently determined crystal structure of the heterotrimeric complex comprising subunits PA, PB1 and PB2 has provided key insights into its mechanism (16, 17). Early work to identify RdRp inhibitory compounds established that the endonuclease activity is an attractive target for influenza drug development (18). Translation of viral mRNAs by the host ribosome requires that they be 5′ capped, and this is achieved in cells infected with influenza virus by a "cap-snatching" mechanism in which the endonuclease cleaves 5′ caps from host mRNAs, which then act as transcription primers (19). The endonuclease domain occupies the N-terminal half of PA (PA_N) (20, 21) and contains a two-metal (Mn^{2+}) active site that preferentially cleaves the pre-mRNA substrate at the 3′ end of a guanine located 12 nucleotides from the 5′ cap (22). The active site is well conserved (23), and crystal structures have revealed how it

Significance

The endonuclease domain within the influenza virus heterotrimeric replication machinery is essential and represents an attractive drug target. It is important to understand the structural basis of potential inhibitor resistance, to design appropriate inhibitors and to prioritize drug candidates that are unlikely to cause the rapid development of clinically-relevant resistance mutations. Using a prototypical endonuclease inhibitor (L-742,001), we used mutagenesis to select for replication competent resistant mutants and studied the structural and functional basis for the observed resistance. These studies confirm that the endonuclease domain is an excellent drug target for treating influenza. They also provide reagents (mutant viruses and constructs) and crucial pharmacophore knowledge that will aid in the development of new drug candidates for urgently needed influenza therapies.

Author contributions: M.-S.S., G.K., T.R.W., R.J.W., and S.W.W. designed research; M.-S.S., G.K., W.R.S., W.Z., T.J., Z.L., P.J.S., T.P.F., and S.-W.Y. performed research; M.-S.S., G.K., W.R.S., W.Z., T.R.W., R.J.W., and S.W.W. analyzed data; M.-S.S., G.K., W.R.S., W.Z., T.R.W., R.J.W., and S.W.W. wrote the paper; T.R.W. oversaw medicinal chemistry; R.J.W. oversaw virology; and S.W.W. oversaw structural biology.

The authors declare no conflict of interest.

This article is a PNAS Direct Submission. S.C. is a guest editor invited by the Editorial Board.

Freely available online through the PNAS open access option.

Data deposition: Crystallography, atomic coordinates, and structure factors have been deposited in the Protein Data Bank, www.pdb.org (PDB IDs 5DES, 5CGV, 5CCY, 5CL0, 5D2O, 5D42, 5D4G, 5D9J, 5CZN, 5D8U, 5DBS, and 5DEB).

[1]M.-S.S. and G.K. contributed equally to this work.

[2]Present address: College of Medicine and Medical Research Institute, Chungbuk National University, 361-763 Cheongju, Republic of Korea.

[3]To whom correspondence may be addressed. Email: Stephen.white@stjude.org, richard.webby@stjude.org, or thomas.webb@sri.com.

This article contains supporting information online at www.pnas.org/lookup/suppl/doi:10.1073/pnas.1519772113/-/DCSupplemental.

engages the centrally bound nucleotide of the substrate (24). Recent studies revealed how inhibitory compounds engage the active site (24–26).

In the case of HIV and HCV, the development of single-agent drug associated resistance via Darwinian selection was observed early in the drug discovery process. The error-prone nature of influenza viral replication can likewise rapidly generate point mutants for the selection of resistance that have seriously compromised the efficacy of influenza therapeutics (27). Here we have investigated this phenomenon with respect to compounds that target the influenza virus endonuclease domain. We used the inhibitor L-742,001, a 4-substituted 2,4-dioxobutanoic acid that effectively inhibits viral growth in both cell culture and mouse models (18, 28, 29). We recently confirmed that L-742,001 inhibits the activity of the isolated endonuclease domain and structurally characterized its binding at the active site (26). Here, we demonstrate that resistant mutations do not emerge by simply passaging the virus repeatedly in the presence of the compound. Viruses with reduced sensitivity were only observed after randomly introducing mutations into the endonuclease domain and then selecting for viable strains in the presence of the inhibitor. Four mutations within the endonuclease active site are able to generate resistance while maintaining viral fitness. These results confirm that L-742,001 indeed targets the endonuclease within the intact virus and reveal that resistance does not emerge unless the mutational landscape for selection is artificially increased.

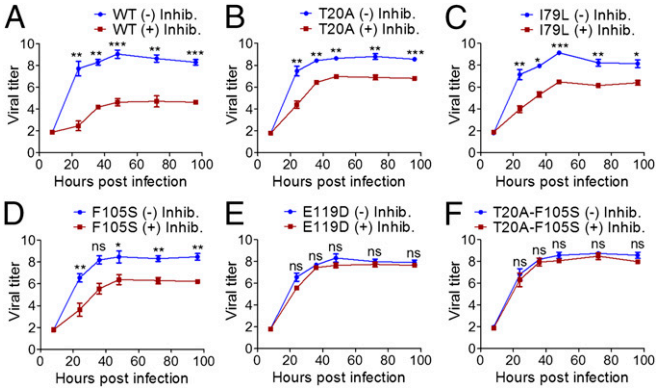

Fig. 1. Impact of endonuclease resistance mutations on the growth of the PR8 influenza virus. A multiplicity of infection (MOI) of 10^{-4} of wild-type (*A*) and PR8 mutant (*B–F*) viruses was used to infect MDCK cells in the presence (red) or absence (blue) of 10 μM of inhibitory compound L-742,001. Supernatants were collected at 8, 24, 36, 48, 72, and 96 h post inoculation and viral titers determined on MDCK cells by using the Reed–Muench 50% endpoint method (47). Virus titers are displayed as log10 50% tissue culture infectious doses ($TCID_{50}$). The limit of virus detection was 1.8 $\log_{10}$ $TCID_{50}$ per mL. Error bars represent SEM derived from three independent experiments. The Student's *t* test was used for statistical comparisons (*$P < 0.05$; ns, not significant).

Results

Selection of Variants Resistant to L-742,001. L-742,001 has a trefoil-like structure and is therefore an ideal molecule to probe the resistance landscape of the rather large endonuclease active site locale. L-742,001 (26) and related compounds (24) engage the central two-metal core and interact with many of the surrounding residues. We initially attempted to obtain resistant variants by passaging wild-type A/Puerto Rico/8/34 (henceforth PR8) virus in the presence of L-742,001 with a gradual increase in inhibitor concentration (10 μM, 20 μM, and 40 μM). After ten passages followed by whole virus genome sequencing, we found only one mutation within the PB2 gene, but viruses containing this mutation remained susceptible to L-742,001 at levels similar to that of the wild-type virus (*SI Appendix*, Table S1 and Fig. S1). Assuming that this approach was too inefficient to generate the necessary pool of selectable mutations, we expanded the diversity by randomly introducing mutations into the endonuclease coding sequence (nucleotides 1–588 of the PA gene) to create a library of "PA_N-rm" plasmids in the reverse genetics vector pHW2000. We sequenced 24 clones from this library and about 42% contained mutations that lead to the truncation of the PA ORF. The remaining clones had between 0 and 11 mutations distributed throughout the domain showing that our approach provided good coverage across the region of interest. This plasmid library was cotransfected with the remaining seven PR8 genes to generate a large pool of PA_N-rm viruses. Five hundred microliters of this pool was then passaged in MDCK cells in the presence of L-742,001 to select for resistant viruses. After three to four passages, the PA genes from resistant viruses were sequenced from all replicates. The sequencing revealed the following point mutations resulting from single nucleotide changes; I79L, E119D, and T20A-F105S.

Functional Impact of the Resistance Mutations. To ensure that all subsequent experiments were conducted with clonal isolates, six PR8 viruses containing wild-type PA_N and PA_N with mutations T20A, I79L, E119D, F105S, or T20A-F105S were generated by reverse genetics (30), and these were compared for susceptibility to L-742,001 in vitro. We first monitored their growth properties in MDCK cells in the presence or absence of 10 μM L-742,001 (Fig. 1). Wild-type PR8 showed a dramatic reduction in viral growth (4–5 $\log_{10}TCID_{50}$/mL decrease in viral titers) in the presence of inhibitor at all time-points. However, the T20A, I79L, and F105S mutants were only mildly affected by the inhibitor (2–3 $\log_{10}TCID_{50}$/mL decrease) and the growth of the E119D and T20A-F105S mutants was completely unaffected by the inhibitor at all time-points. IC_{50} values derived from a plaque inhibition assay showed a similar trend (Table 1). In the absence of inhibitor, there was no significant difference in fitness between the wild-type and mutant viruses (Fig. 1 and *SI Appendix*, Fig. S2*A*). To determine their in vivo viral fitness, 10^4 PFU of the wild-type and mutant viruses were inoculated into mice. Mice infected with wild-type virus lost weight from 2 d post inoculation (dpi) (*SI Appendix*, Fig. S3*A*) and succumbed to infection within seven dpi (*SI Appendix*, Fig. S3*B*). Mice infected with the five mutant viruses all showed similar patterns of weight loss and survival (*SI Appendix*, Fig. S3 *A* and *B*). The mouse LD_{50} values (LD_{50}) of the mutants did not significantly differ from those of the wild-type virus and ranged between 2.2–2.7 MLD_{50} (*SI Appendix*, Fig. S3*B*). Although there were small but significant titer differences between viruses over the course of the study, all viral lung titers peaked between 3 and 5 dpi (6.1–7.3 $\log_{10}TCID_{50}$ per g) and were maintained until 7 dpi (more than 5.5 $\log_{10}TCID_{50}$ per g) (*SI Appendix*, Fig. S4). To confirm that all mutations were maintained during replication in vitro and in vivo, and that no additional changes had taken place during the experiments, cell supernatants and mice lungs at the last time point were collected and sequenced (*SI Appendix*, Table S2).

To directly assess the impact of the identified resistance mutations on polymerase activity, we used a luciferase-based minigenome assay (31). Similar to the results from the viral growth and plaque inhibition assays, the T20A, I79L, and F105S mutations increased resistance to L-742,001 by a modest two- to fivefold compared with wild type whereas E119D and T20A-F105S showed significantly higher resistance values of 29.4- and 10.7-fold, respectively (Fig. 2*A*). The polymerase activities of the mutant viruses in the absence of L-742,001 were all maintained at above 80% of the wild type (Fig. 2*B*).

Phenotypically important mutations in influenza viruses can be genetically context dependent and have different effects in different viruses. To address this issue with the L-742,001 resistance mutations, we introduced I79L, F105S, and E119D into a pandemic H1N1 2009 (A/Tennessee/1–560/2009) virus (pH1N1 henceforth). This virus naturally possesses an alanine at position 20 within the endonuclease domain that was shown to be associated with decreased susceptibility to L-742,001 (29). Consistent with this observation, wild-type pH1N1 virus showed a 7.8-fold higher IC_{50} to L-742,001 than the wild-type PR8 virus (Table 1). The introduction of the three mutations I79L, E119D and F105S increased resistance 2.8-, 4.2-, and 9.7-fold, respectively (Table 1).

Table 1. The L-742,001–resistant variants in the PR8 and pH1N1 virus backgrounds

Strains PR8* and pH1N1†	Mutated residue: Position and identity				IC_{50} (L-742,001)	
	20	79	105	119	Value‡	Ratio§
PR8 PA_{wt}	T	I	F	E	3.13	1.0
PR8 PA_{T20A}	A¶	I	F	E	9.30	3.0
PR8 PA_{I79L}	T	L¶	F	E	7.48	2.4
PR8 PA_{F105S}	T	I	S¶	E	9.63	3.1
PR8 PA_{E119D}	T	I	F	D¶	25.94	8.3
PR8 $PA_{T20A\text{-}F105S}$	A¶	I	S¶	E	34.70	11.1
pH1N1 PA_{wt}	A	I	F	E	24.48	1.0
pH1N1 PA_{I79L}	A	L¶	F	E	68.30	2.8
pH1N1 PA_{E119D}	A	I	F	**D**¶	102.60	4.2
pH1N1 PA_{F105S}	A	I	**S**¶	E	236.50	9.7

Results from plaque inhibition assays.
*A/Puerto Rico/8/34 influenza virus.
†Pandemic H1N1 2009 (A/Tennessee/1–560/2009) influenza virus.
‡Values in μM.
§Normalized with respect to the inhibition of wild-type viruses.
¶The indicated mutations were introduced into the PA_N domain of the reconstructed virus background. The two in bold were further characterized by kinetics and structural studies.

Similar to the PR8 virus, there was no significant difference in fitness between the wild-type and mutant viruses in the absence of inhibitor (*SI Appendix*, Fig. S2*B*).

Kinetic and Structural Analyses of the Wild-Type Endonuclease. Studies by others (24) have shown that the endonuclease domain from pH1N1 yields superior crystal structures of inhibitor complexes than the A/Vietnam/1203/2004 (H5N1) strain that we previously studied (26). Having demonstrated that the selected resistance mutations are also effective in the pH1N1, we switched to this strain for our kinetic, binding and structural analyses of the resistance mutants. We specifically used the PA_N domain from A/California/04/2009, which is genetically very similar to A/Tennessee/1–560/2009, and created the construct $PA_N^{\Delta Loop}$. This construct is similar to that previously studied (24) apart from a nonessential flexible loop (residues 51–72) that was deleted in our previous studies (26). Crystals of this construct routinely produced apo and complex structures at 2.3 Å resolution or better (*SI Appendix*, Tables S3–S5).

Using a previously developed FRET-based assay (20, 32), we first confirmed that $PA_N^{\Delta Loop}$ has a robust nuclease activity. Fig. 3*A* shows the Michaelis–Menten curve using 200 nM of protein, and *SI Appendix*, Fig. S5*A* shows the full kinetic analysis from which V_{max} and K_M values of 3764190 s^{-1} and 1566 nM, respectively, were derived. We then measured the binding of our fluorescent probe (25) to $PA_N^{\Delta Loop}$ by fluorescent polarization, and the K_d was found to be 44 nM (Fig. 3*B*). We also used L-742,001 to remove the prebound probe (Fig. 3*C*) and measured IC_{50} and K_i values of 0.89 μM and 0.34 μM, respectively.

Finally, we structurally characterized the interaction of $PA_N^{\Delta Loop}$ with the mononucleotides dTMP and rUMP (*SI Appendix*, Fig. S6), and with L-742,001 (Fig. 4 *A* and *D*). The mononucleotides bind in the same manner as previously reported (24) with the phosphate group interacting with the paired Mn^{2+} ions and the base engaging the side chains of Tyr24 and Lys34. L-742,001 engages the active site in the same manner as the related compound R05-2 (24), with the *p*-chlorobenzene arm forming a stacking interaction with Phe105 and the phenyl arm engaging Ala20, Tyr24, and Ile38. This is a key result because our previously reported L-742,001 complex structure using the endonuclease from H5N1 showed significant differences (26).

Kinetic and Structural Analyses of the Resistant Endonucleases. The I79L mutation generated minimal resistance to L-742,001 in both the PR8 and pH1N1 strains and we therefore focused on the F105S and E119D mutations. These were individually introduced into the $PA_N^{\Delta Loop}$ construct that naturally contains the T20A substitution. The kinetic assay revealed that F105S is only marginally impaired compared with the wild-type enzyme whereas E119D is seriously impaired (Fig. 3*A* and *SI Appendix*, Fig. S5 *B* and *C*). The V_{max} values were calculated as 2854244 and 537470 s^{-1} (76% and 14%, respectively, of the wild-type values). The K_M value for F105S was slightly increased (2645 nM) but we were unable to estimate the K_M for E119D. Binding studies using the fluorescent probe (Fig. 3*B*) also showed the greatest effect with E119D. The K_d with E119D (949 nM) was ∼20 times larger than that of the wild-type protein, whereas the K_d value for F105S was largely unaffected (22 nM). The IC_{50} and K_i values for F105S derived from the probe displacement assay (Fig. 3*C*) were similar to the wild-type (1.49 μM and 0.39 μM, respectively), but much higher with E119D (7.08 μM and 1.98 μM).

We then addressed the impact of the F105S (Fig. 5*A* and *SI Appendix*, Fig. S7*A*) and E119D (Fig. 5*B* and *SI Appendix*, Fig. S7*B*) mutations on the $PA_N^{\Delta Loop}$ structure. Both structures are very similar to the wild-type structure, but a significant difference in the E119D protein is the loss of an active site Mn^{2+} ion. The "proximal" Mn^{2+} ion coordinated by His41, Asp108, Asp119, and Ile120 is present, but the "distal" Mn^{2+} coordinated by Glu80 and Asp108 is missing. The crystal structures of F105S and E119D in complex with mononucleotides were also determined. F105S in complex with dTMP and rUMP are identical to the wild-type complexes with both Mn^{2+} ions present (Fig. 5*C* and *SI Appendix*, Fig. S7 *C* and *E*). However, the two E119D complexes showed significant differences (Fig. 5*D* and *SI Appendix*, Fig. S7 *D* and *F*). Although the rUMP complex is very similar to that of the wild type, the distal Mn^{2+} ion only became visible in the presence of 10-fold higher concentrations of metal (50 mM $MnCl_2$ and $MgCl_2$) and substrate (200 mM rUMP). In the dTMP complex, the distal Mn^{2+} ion is never present and the nucleotide phosphate group compensates by moving to displace a water molecule and form a hydrogen bond with the main chain amino group of Val122. Perhaps as a result of this movement, the base no longer engages Tyr24 but moves to occupy a different pocket surrounded by Lys34, Ala37, Val122, and Arg124.

The crystal structures of the mutant proteins in complex with L-742,001 were also resolved. Although the inhibitor is clearly present in both structures, no electron density was observed for the phenyl arm, presumably due to free rotation of this group. The electron density for the phenyl arm was not seen even at higher concentrations of the inhibitor in the crystallization solution. In the

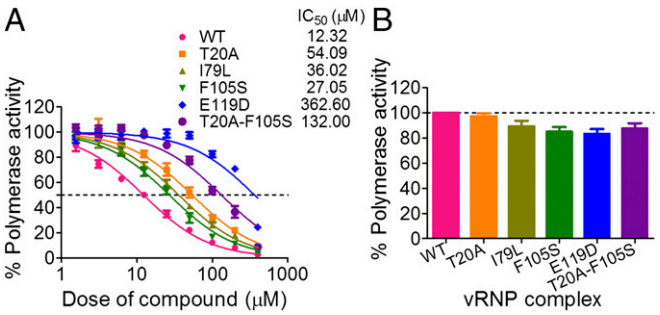

Fig. 2. The PR8 viral polymerase: impact of endonuclease resistance mutations on susceptibility to L-742,001 and activity. Polymerase activity was monitored in the presence of L-742,001 (*A*) and in the absence of L-742,001 (*B*). In *A*, the inhibitor was added at 6 h after transfection in dose dependent manner and the 50% polymerase inhibitory concentrations (IC_{50}s) are indicated. In *B*, the signal is shown relative to the wild-type complex. Data shown are the means ± SEM from at least three independent tests. See text for details of the firefly minigenome luciferase assay.

PHARMACOLOGY

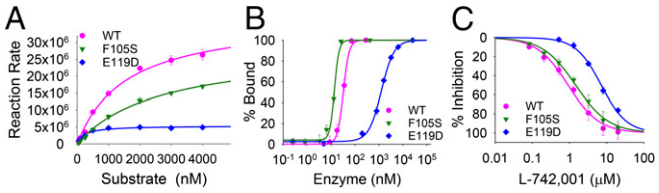

Fig. 3. Kinetic and inhibitor binding studies of the wild-type, F105S, and E119D RdRp endonuclease domains from influenza strain A/California/04/2009. (*A*) Michaelis–Menten plot at 200 nM of endonuclease. The reaction rates are shown as relative fluorescence units (RFU) per hour. The full Michaelis–Menten kinetic analysis is presented in *SI Appendix*, Fig. S5. (*B*) Percent binding of the fluorescent probe (25) to the endonuclease domain as monitored by fluorescence polarization. Probe (60 nM) was used with increasing concentrations of protein. (*C*) Dose dependent displacement of the fluorescent probe from the endonuclease domain by L-742,001. Probe concentration was 60 nM, and the protein concentration was based on 85% (IC_{85}) binding saturation (*B*). The dose–response curves were fitted with four parameter logistic curves, and the K_i values were calculated from the corresponding IC_{50} values.

F105S complex (Fig. 4 *B* and *E*), the loss of the Phe105 side chain removes the key stacking interaction with the *p*-chlorobenzene arm that relocates to a new position adjacent to Lys34. In the E119D complex (Fig. 4 *C* and *F*), the *p*-chlorobenzene arm occupies the wild-type location adjacent to Phe105, but the phenyl arm remains disordered despite its binding pocket adjacent to Tyr24 being available. The reason may be a decrease in the binding affinity of Mn^{2+} ions leading to destabilization of the stacking interaction of the phenyl group with Tyr24. In the case of the E119D complex with rUMP, both Mn^{2+} ions were only observed at a 10-fold higher concentration of $MnCl_2$ and $MgCl_2$. The apparent ease by which the two similar arms of L-742,001 can rotate and occupy different pockets within the open active site in response to these mutations while maintaining the interaction of the diketo moiety with the two-metal site may explain why the compound adopts a different conformation in pH1N1 (Fig. 4*B*) compared with H5N1 (26).

Discussion

Current antiinfluenza drugs target the M2 ion channel (amantadine and rimantadine) and the neuraminidase (zanamivir and oseltamivir), but the rapid emergence of resistant strains has severely reduced their clinical usefulness (33, 34). Structural studies have now revealed new opportunities for drug discovery that target the essential endonuclease activity of the virus (24–26). In the current study, we had two primary goals; to confirm that the known endonuclease inhibitor L-742,001 targets the enzyme within the intact virus by generating resistant mutants, and to survey the resistance potential of the endonuclease by characterizing the sites of mutation. We failed to generate viable resistant viruses using traditional in vitro approaches, but succeeded by developing a directed mutagenesis approach. Four resistance mutations were identified, T20A, I79L, F105S, and E119D, and all map to the endonuclease active site thereby confirming it as the target of L-742,001. These mutations partially overlap with those identified in an earlier L-742,001 study (35), and elicited resistance in both of the influenza strains tested.

Structural analyses of the wild-type and mutant pH1N1 endonuclease domains with and without bound L-742,001 revealed how these mutations compromise drug binding. Phe105 interacts with the *p*-chlorobenzene arm of L-742,001, and its mutation to serine presumably reduces the binding affinity. The resistance effect of F105S in strain PR8 is increased by the additional T20A mutation. T20A may not be a bona fide resistant mutation because over 98% of deposited sequences harbor this variation (*SI Appendix*, Table S6). Nonetheless, alanine provides a selective advantage when L-742,001 is present and T20A was also identified in the earlier studies (35). This residue is located on the opposite side of the active site to Phe105, and they may act in concert to influence the positioning of the *p*-chlorobenzene and phenyl arms of L-742,001 (Fig. 4*A*). Glu119 contributes to the coordination shells of the two Mn^{2+} ions, directly to the proximal Mn^{2+} ion and indirectly via a water molecule to the distal Mn^{2+} ion. The mutation appears to adjust the two-metal coordination geometry and weaken the binding of the distal Mn^{2+}. The distal and proximal Mn^{2+} ions are coordinated by two and four side chains, respectively, which explains their different binding affinities (24). As regards the I79L mutation, this residue is adjacent to the two-metal locale and can potentially impact its conformation.

The two major resistance mutations that we identified were F105S and E119D. F105S is the weaker of the two in terms of its impact on the binding of L-742,001 and its sensitivity to inhibition by the compound. F105S is also the least catalytically impaired enzyme, consistent with its lack of interaction with the mononucleotide at the active site (*SI Appendix*, Fig. S6). E119D generates the least active enzyme, consistent with its role in coordinating the proximal Mn^{2+} ion, and the aspartic acid replacement is clearly unable to efficiently fulfill this role. Surprisingly, these two mutations had a less than anticipated impact on viral replication in cells and mice, although the more defective E119D did have the lowest titers at the conclusion of both infection experiments (Fig. 1*E* and *SI Appendix*, Figs. S2 and S4). Thus, the compromised endonuclease activities of F105S and E119D when measured with PA in isolation are less apparent in terms of viral fitness in the absence of L-742,001. During infection, both mutations evidently permit adequate levels of catalytic activity for viral replication while selectively disfavoring inhibitor binding. One explanation, supported by the polymerase assay (Fig. 2*B*) and the structure of the heterotrimeric (16, 17), is that the mutations have less effect in the context of the intact RdRp complex where the RNA substrate is also bound by the CAP-binding domain.

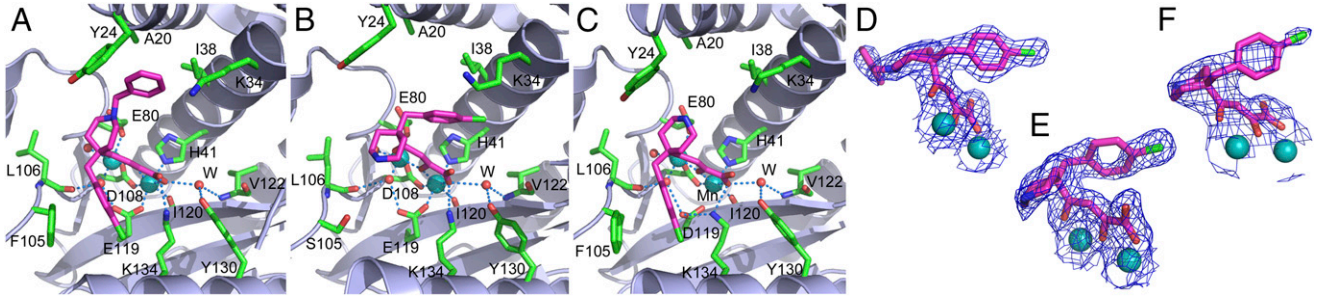

Fig. 4. Crystal structures of the L-742,001 inhibitor in complex with the RdRp endonuclease domain from the pandemic H1N1 2009 influenza virus (construct $PA_N^{\Delta Loop}$). (*A*) Wild-type endonuclease. (*B*) F105S. (*C*) E119D. In each figure, the protein secondary structure is shown as a cartoon in gray/blue, amino acids are shown in stick representation with green carbons, L-742,001 is shown in stick with pink carbons, water molecules are shown as red spheres, and metal ions are shown as teal spheres. Hydrogen bonds and metal coordination are displayed by dashed lines. *D*, *E*, and *F* show the 2Fo-Fc electron densities for L-742,001 in *A*, *B*, and *C*, respectively, contoured at 1 σ.

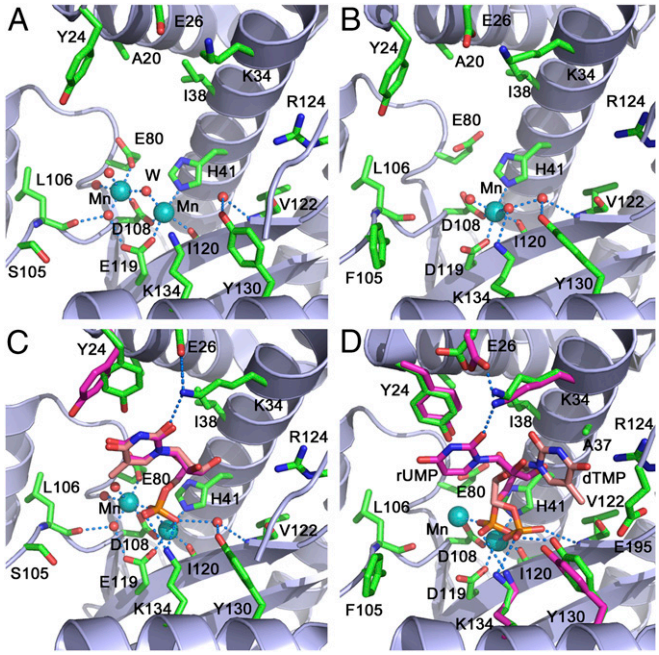

Fig. 5. Crystal structures of the apo and nucleotide-bound mutant PA endonuclease domains from the pH1N1 influenza virus (construct $PA_N^{\Delta Loop}$). (*A*) apo F105S mutant. (*B*) apo E119D. (*C*) F105S in complex with dTMP/rUMP. (*D*) E119D in complex with dTMP/rUMP. In each figure, the protein secondary structure is shown in gray/blue, amino acids in stick representation with green carbons, water molecules as red spheres, and metal ions as teal spheres. In *C* and *D*, the two substrate-bound structures are superimposed. The amino acids with green carbons correspond to the rUMP (peach carbons) complex structure, and those with pink carbons correspond to the dTMP (also pink carbons) complex. In the F105S complexes (*C*), the structures are almost identical apart from the orientation of Tyr24. In the E119D complexes (*D*), there are substantial differences between the two structures. Hydrogen bonds and metal coordination are displayed by dashed lines. The electron densities are shown in *SI Appendix*, Fig. S7.

Overall, our studies support the notion that the endonuclease domain is an attractive target for influenza antiviral drug discovery. Although we were able to generate resistant viruses synthetically, it was not possible to induce resistant mutations to L-742,001 in wild-type virus even after 10 passages in the presence of the compound. In contrast, viruses resistant to adamantanes and neuraminidase inhibitors can be readily generated using this approach (36–40). Although it is encouraging that resistance appears difficult to generate naturally, the relatively minor impact on viral fitness of the F105S and E119D mutations does raise caution as to whether resistant viruses would have the capacity for community spread if they were to develop under extended drug pressure. Tempering this concern is the fact that Phe105 and Glu119 are highly conserved and account for greater than 99.5% of all human and avian influenza viruses (41) (*SI Appendix*, Table S6), suggesting that these residues have a selection pressure acting upon them that favors their retention. The evolution of viral strains is a complex process, and it is well established that even a modest reduction in the relative fitness of a mutation can lead to the extinction, or near extinction, of a less fit mutant viral strain (42). Thus, the slightly reduced replication of viruses containing E119D might be critical in the context of competition with wild-type strains when drug pressure is removed. Similarly, the use of more sensitive fitness models, such as ferret transmission, may identify fitness costs of the F105S substitution that we were unable to detect here. Regardless and reflecting the importance of our studies, the FDA has provided guidelines on the preclinical and clinical monitoring of influenza drugs that are under development in regard to potential resistance development (www.fda.gov/downloads/drugs/guidancecomplianceregulatoryinformation/guidances/ucm091219.pdf). These guidelines also suggest that the future treatment of influenza will benefit from a "mixture" of drugs targeting multiple therapeutic vulnerabilities of influenza. Combination drug treatment has been highly effective in the clinical management of HIV and hepatitis C (12, 13).

L-742,001 was ultimately found to be unsuitable for drug development. However, with the availability of effective endonuclease assays and high resolution crystal structures, there have been numerous reports of novel chemotypes that inhibit this enzyme and an upsurge in accompanying medicinal chemistry (43–46). Our studies have revealed some of the structural origins of how resistance can emerge, and this information can now guide medicinal chemists in their optimization of new inhibitor scaffolds and prioritization of early lead compounds. For example, inhibitors that make critical contacts around Phe105 and Glu119 should not be highly ranked in the lead optimization process. In this way, the identified resistance mutations can be used to guide future drug discovery efforts and to design and select compounds that are less prone to the development of drug resistance. In addition, our approach of using random mutagenesis to identify resistance mutations and then introducing them into intact viruses and expression constructs for screening will be invaluable to all researchers in field of antiviral drug discovery.

Experimental Procedures

Additional experimental procedures are available in *SI Appendix*.

Random Mutagenesis. The coding region of the 196 residue PR8 virus endonuclease domain within the RdRp PA subunit gene was randomly mutated using the GeneMorph II EZClone Domain Mutagenesis kit (Stratagene), and the resulting PCR-based plasmid library was transformed into competent cells (DH5α, Invitrogen). Mutations within the library were confirmed by sequencing representative clones. Three plasmid libraries were generated and independently used to rescue viruses.

Selection of Resistant Variants and Reverse Genetics. PR8 variants containing random mutations in the PA endonuclease domain were generated as described (30). Variants that displayed growth in the presence of high doses of the compound were sequenced within the endonuclease domain of the PA gene. The identified mutations were then introduced into the wild-type PA gene by site directed mutagenesis. The same mutations were also introduced into the TN09 virus. Reverse genetically generated wild-type viruses (PR8 and TN09) were used as the control in each case. All rescued viruses were sequenced to confirm that there are no additional mutations elsewhere in the genome.

Viral Polymerase Inhibition Assay. vRNPs, NP-, PA-, PB1-, and PB2-pHW2000 were cotransfected with the firefly luciferase reporter and a β-galactosidase plasmid into 293T cells using TransIT-LT1 (Mirus) and the manufacturer's protocols. For inhibition of polymerase activity by L-742,001, 0–400 μM of the compound were added at 6 h after transfection. After 24 h incubation at 37 °C, luciferase activity was determined (Promega) and normalized against the β-galactosidase activity level of the cells. The IC_{50} was calculated as the compound concentration causing 50% reduction of luciferase signal using Prism software (Prism 5.0).

Viral Growth Kinetics in Vitro. A multiplicity of infection (MOI) of 10^{-4} of PR8 variants and wild-type were infected to MDCK cells to compare their growth kinetics. Supernatants were collected at 8, 24, 36, 48, 72, and 96 h post inoculation for virus titration and endpoint-titrated by the 50% tissue culture infectious doses ($TCID_{50}$) of viruses in MDCK cells (47). The limit of virus detection was 1.8 $\log_{10}$ $TCID_{50}$/mL and Student's *t* test was used for statistical comparisons ($P < 0.05$) and calculated by using Prism 5.0.

In Vivo Characterization. Groups of 20 6-wk-old female BALB/c mice were lightly anesthetized by isoflouran and inoculated intranasally with 10^4 PFU of viruses. Virus infected mice were monitored for up to 13 d for weight change and mortality, and three mice from each group were euthanized at 1, 3, 5, 7, and 9 dpi for lung viral titrations. The mice lungs were subjected to titer by $TCID_{50}$/mL in MDCK cells. When the mice lost 25% or more of their initial body weight, they were euthanized. The LD_{50}s in mice (MLD_{50}s) were determined in 10-fold serial dilution groups (10^2 to 10^6 $TCID_{50}$ per 50 μL) (47).

Cloning, Overexpression, and Protein Purification. A loop-deleted version of PA_N from pandemic H1N1 influenza virus A/Tennessee/1–560/2009, in which residues 51–72 were replaced with the three-residue linker sequence GGS,

PHARMACOLOGY

was cloned with a C-terminal 10xHis tag as described earlier (26). We refer to this construct as $PA_N^{\Delta Loop}$. Two derivative clones containing the point mutations F105S and E119D were created by site-directed mutagenesis. The three proteins were expressed using BL21(DE3) cells, and purified by affinity chromatography and gel filtration. For E119D, it subsequently proved necessary to move the 10xHis tag to the N terminus.

Nuclease Activity and Fluorescence Polarization Binding Assays. We followed previously developed procedures for both assays. For the FRET-based activity assay, the substrate is 5′-Cy5-GAATACTCAAGCTATGCATC-3IAbRQSp (20, 32). Details of our fluorescent binding probe and the fluorescent polarization assay have been described (25).

Crystallographic Analyses. Crystallization screening was carried out at 18 °C using the Phoenix crystallization robot (Art Robbins Instruments). Crystals of the various complexes were obtained by soaking apo crystals in mother liquor supplemented with the ligand and $MnCl_2$/$MgCl_2$. Diffraction data were collected from cryo-protected crystals at the SERCAT 22-ID or 22-BM beam lines at the Advanced Photon Source. Data sets were indexed, integrated, and scaled using HKL2000 (48), and the structures were determined by molecular replacement and refined using the CCP4 suite (49). Model building and refinement was conducted using Coot (50). For data collection and refinement statistics, see *SI Appendix*, Tables S3–S5.

ACKNOWLEDGMENTS. We thank Robert Webster, Mi-Kyung Yun, Darcie Miller, and John Bollinger for their assistance. Diffraction data were collected at Southeast Regional Collaborative Access Team (SERCAT) beam lines 22-ID and 22-BM at the Advanced Photon Source (APS), Argonne National Laboratory. Supporting SERCAT institutions may be found at www.ser-cat.org/members.html. Use of the APS is supported by the US Department of Energy under Contract W-31-109-Eng-38. This work was supported by NIH Grant AI098757 (to T.R.W.), Cancer Center Core Grant CA21765, Centers of Excellence for Influenza Research and Surveillance Contracts HHSN266200700005C and HHSN272201400006C, and the American Lebanese Syrian Associated Charities (ALSAC).

1. Webster RG, Bean WJ, Gorman OT, Chambers TM, Kawaoka Y (1992) Evolution and ecology of influenza A viruses. *Microbiol Rev* 56(1):152–179.
2. Thompson WW, et al. (2003) Mortality associated with influenza and respiratory syncytial virus in the United States. *JAMA* 289(2):179–186.
3. Beyer WE, et al. (2013) Cochrane re-arranged: Support for policies to vaccinate elderly people against influenza. *Vaccine* 31(50):6030–6033.
4. Osterholm MT, Kelley NS, Sommer A, Belongia EA (2012) Efficacy and effectiveness of influenza vaccines: A systematic review and meta-analysis. *Lancet Infect Dis* 12(1): 36–44.
5. Dwyer DE; INSIGHT Influenza Study Group (2011) Surveillance of illness associated with pandemic (H1N1) 2009 virus infection among adults using a global clinical site network approach: The INSIGHT FLU 002 and FLU 003 studies. *Vaccine* 29(Suppl 2): B56–B62.
6. Taubenberger JK, Reid AH, Krafft AE, Bijwaard KE, Fanning TG (1997) Initial genetic characterization of the 1918 "Spanish" influenza virus. *Science* 275(5307):1793–1796.
7. Garten RJ, et al. (2009) Antigenic and genetic characteristics of swine-origin 2009 A (H1N1) influenza viruses circulating in humans. *Science* 325(5937):197–201.
8. Li Q, et al. (2014) Epidemiology of human infections with avian influenza A(H7N9) virus in China. *N Engl J Med* 370(6):520–532.
9. Van Kerkhove MD (2013) Brief literature review for the WHO global influenza research agenda–highly pathogenic avian influenza H5N1 risk in humans. *Influenza Other Respi Viruses* 7(Suppl 2):26–33.
10. Herfst S, et al. (2012) Airborne transmission of influenza A/H5N1 virus between ferrets. *Science* 336(6088):1534–1541.
11. Imai M, et al. (2012) Experimental adaptation of an influenza H5 HA confers respiratory droplet transmission to a reassortant H5 HA/H1N1 virus in ferrets. *Nature* 486(7403):420–428.
12. Sgarbanti M, Battistini A (2013) Therapeutics for HIV-1 reactivation from latency. *Curr Opin Virol* 3(4):394–401.
13. Scheel TK, Rice CM (2013) Understanding the hepatitis C virus life cycle paves the way for highly effective therapies. *Nat Med* 19(7):837–849.
14. Fodor E (2013) The RNA polymerase of influenza a virus: Mechanisms of viral transcription and replication. *Acta Virol* 57(2):113–122.
15. Resa-Infante P, Jorba N, Coloma R, Ortin J (2011) The influenza virus RNA synthesis machine: Advances in its structure and function. *RNA Biol* 8(2):207–215.
16. Pflug A, Guilligay D, Reich S, Cusack S (2014) Structure of influenza A polymerase bound to the viral RNA promoter. *Nature* 516(7531):355–360.
17. Reich S, et al. (2014) Structural insight into cap-snatching and RNA synthesis by influenza polymerase. *Nature* 516(7531):361–366.
18. Tomassini J, et al. (1994) Inhibition of cap (m7GpppXm)-dependent endonuclease of influenza virus by 4-substituted 2,4-dioxobutanoic acid compounds. *Antimicrob Agents Chemother* 38(12):2827–2837.
19. Plotch SJ, Bouloy M, Ulmanen I, Krug RM (1981) A unique cap(m7GpppXm)-dependent influenza virion endonuclease cleaves capped RNAs to generate the primers that initiate viral RNA transcription. *Cell* 23(3):847–858.
20. Dias A, et al. (2009) The cap-snatching endonuclease of influenza virus polymerase resides in the PA subunit. *Nature* 458(7240):914–918.
21. Yuan P, et al. (2009) Crystal structure of an avian influenza polymerase PA(N) reveals an endonuclease active site. *Nature* 458(7240):909–913.
22. Datta K, Wolkerstorfer A, Szolar OH, Cusack S, Klumpp K (2013) Characterization of PA-N terminal domain of Influenza A polymerase reveals sequence specific RNA cleavage. *Nucleic Acids Res* 41(17):8289–8299.
23. Crépin T, et al. (2010) Mutational and metal binding analysis of the endonuclease domain of the influenza virus polymerase PA subunit. *J Virol* 84(18):9096–9104.
24. Kowalinski E, et al. (2012) Structural analysis of specific metal chelating inhibitor binding to the endonuclease domain of influenza pH1N1 (2009) polymerase. *PLoS Pathog* 8(8):e1002831.
25. Baughman BM, et al. (2012) Identification of influenza endonuclease inhibitors using a novel fluorescence polarization assay. *ACS Chem Biol* 7(3):526–534.
26. DuBois RM, et al. (2012) Structural and biochemical basis for development of influenza virus inhibitors targeting the PA endonuclease. *PLoS Pathog* 8(8):e1002830.
27. Hurt AC (2014) The epidemiology and spread of drug resistant human influenza viruses. *Curr Opin Virol* 8:22–29.
28. Hastings JC, Selnick H, Wolanski B, Tomassini JE (1996) Anti-influenza virus activities of 4-substituted 2,4-dioxobutanoic acid inhibitors. *Antimicrob Agents Chemother* 40(5):1304–1307.
29. Nakazawa M, et al. (2008) PA subunit of RNA polymerase as a promising target for anti-influenza virus agents. *Antiviral Res* 78(3):194–201.
30. Hoffmann E, Neumann G, Kawaoka Y, Hobom G, Webster RG (2000) A DNA transfection system for generation of influenza A virus from eight plasmids. *Proc Natl Acad Sci USA* 97(11):6108–6113.
31. Salomon R, et al. (2006) The polymerase complex genes contribute to the high virulence of the human H5N1 influenza virus isolate A/Vietnam/1203/04. *J Exp Med* 203(3):689–697.
32. Noble E, Cox A, Deval J, Kim B (2012) Endonuclease substrate selectivity characterized with full-length PA of influenza A virus polymerase. *Virology* 433(1):27–34.
33. Barr IG, et al.; Writing Committee of the World Health Organization Consultation on Northern Hemisphere Influenza Vaccine Composition for 2013–2014 (2014) WHO recommendations for the viruses used in the 2013-2014 Northern Hemisphere influenza vaccine: Epidemiology, antigenic and genetic characteristics of influenza A(H1N1)pdm09, A(H3N2) and B influenza viruses collected from October 2012 to January 2013. *Vaccine* 32(37):4713–4725.
34. Hauge SH, Dudman S, Borgen K, Lackenby A, Hungnes O (2009) Oseltamivir-resistant influenza viruses A (H1N1), Norway, 2007-08. *Emerg Infect Dis* 15(2):155–162.
35. Stevaert A, et al. (2013) Mutational analysis of the binding pockets of the diketo acid inhibitor L-742,001 in the influenza virus PA endonuclease. *J Virol* 87(19):10524–10538.
36. Hay AJ, Wolstenholme AJ, Skehel JJ, Smith MH (1985) The molecular basis of the specific anti-influenza action of amantadine. *EMBO J* 4(11):3021–3024.
37. Gubareva LV, et al. (1996) Characterization of mutants of influenza A virus selected with the neuraminidase inhibitor 4-guanidino-Neu5Ac2en. *J Virol* 70(3):1818–1827.
38. McKimm-Breschkin JL (2000) Resistance of influenza viruses to neuraminidase inhibitors–a review. *Antiviral Res* 47(1):1–17.
39. Ilyushina NA, Bovin NV, Webster RG, Govorkova EA (2006) Combination chemotherapy, a potential strategy for reducing the emergence of drug-resistant influenza A variants. *Antiviral Res* 70(3):121–131.
40. Hurt AC, Holien JK, Barr IG (2009) In vitro generation of neuraminidase inhibitor resistance in A(H5N1) influenza viruses. *Antimicrob Agents Chemother* 53(10):4433–4440.
41. Squires RB, et al. (2012) Influenza research database: An integrated bioinformatics resource for influenza research and surveillance. *Influenza Other Respi Viruses* 6(6):404–416.
42. Aguirre J, Lázaro E, Manrubia SC (2009) A trade-off between neutrality and adaptability limits the optimization of viral quasispecies. *J Theor Biol* 261(1):148–155.
43. Sagong HY, et al. (2013) 3-Hydroxyquinolin-2(1H)-ones As Inhibitors of Influenza A Endonuclease. *ACS Med Chem Lett* 4(6):547–550.
44. Sagong HY, et al. (2014) Phenyl substituted 4-hydroxypyridazin-3(2H)-ones and 5-hydroxypyrimidin-4(3H)-ones: Inhibitors of influenza A endonuclease. *J Med Chem* 57(19):8086–8098.
45. Carcelli M, et al. (2014) Metal-chelating 2-hydroxyphenyl amide pharmacophore for inhibition of influenza virus endonuclease. *Mol Pharm* 11(1):304–316.
46. Fudo S, et al. (2015) Structural and computational study on inhibitory compounds for endonuclease activity of influenza virus polymerase. *Bioorg Med Chem* 23(17): 5466–5475.
47. Reed LJ, Muench H (1938) A simple method of estimating fifty percent endoints. *Am J Hyg* 27:493–497.
48. Otwinowski Z, Minor W (1997) Processing of X-ray diffraction data collected in oscillation mode. *Methods Enzymol* 276:307–326.
49. Winn MD, et al. (2011) Overview of the CCP4 suite and current developments. *Acta Crystallogr D Biol Crystallogr* 67(Pt 4):235–242.
50. Emsley P, Cowtan K (2004) Coot: Model-building tools for molecular graphics. *Acta Crystallogr D Biol Crystallogr* 60(Pt 12 Pt 1):2126–2132.